A Photometric Study of the Eclipsing Binary Star BN Ari

Edward J. Michaels
Stephen F. Austin State University, Department of Physics and Astronomy, P.O. Box 13044, Nacogdoches, TX 75962; emichaels@sfasu.edu

Received November 3, 2015; revised November 19, 2015; accepted December 8, 2015

Abstract Presented are a set of multi-band light curves, synthetic light curve solutions, and period study for the eclipsing binary star BN Ari. The orbital period was found to be decreasing the past 8 years (~8,200 orbits). The observed light curves were analyzed with the Wilson-Devinney program. The resulting synthetic light curve solution showed the system to be a contact eclipsing binary with total eclipses.

1. Introduction

The variability of BN Ari (GSC 1761-1934, TYC 1761-1934-1) was discovered by Otero *et al.* (2004) in the public data release from the Northern Sky Variability Survey (NSVS) (Wozniak 2004) and in the All-Sky Automated Survey (ASAS) data by Pojmański *et al.* (2005). Otero classified the star as an EW/KW type eclipsing binary system and Pojmański as a contact binary (EC) with a period of P = 0.299377 day. Pojmański gives a V-band magnitude of 10.36 for BN Ari with the amplitude of variation as 0.73. Times of minimum light have been reported by a number of observers and will be discussed in the period analysis section of this paper. In this paper a photometric study of BN Ari is presented. It is organized into sections with the observations and data reduction techniques presented in section 2 and new times of minima and a period study presented in section 3. Light curve analysis using BINARY MAKER 3.0 (BM3) (Bradstreet and Steelman 2002) and the Wilson-Devinney model (WD) (Wilson and Devinney 1971; Wilson 1990, 1994; Van Hamme and Wilson 1998) is presented in section 4. Discussion and conclusions are presented in section 5.

2. Observations

BN Ari was observed in the Johnson B and V and Sloan g', r', and i' filter bands using the 0.31-m Ritchey-Chrétien robotic telescope at the Waffelow Creek Observatory (http://obs.ejmj.net/index.php). Images were acquired with an SBIG-STXL camera with a KAF-6303E CCD (9µm pixels) using 2 × 2 on-chip binning to provide faster readout times and proper sampling. Images were taken in 2014 on October 15, 17, 18, 20, 21, 23, 25, 26, 29, 30, and 31 in 5 passbands: 771 images in B, 1128 in V, 1363 in g', 1,076 in r', and 1,156 in i'. These dates comprise the first data set (DS1) and were analyzed using synthetic light curve modeling in section 4. Additional images were acquired in 2014 on November 8, 9, 18, 19, 23, 25, 26, 27, and more recently in 2015 on September 4, 12, 16. These observations comprise a second data set (DS2) in which only one passband was observed each night to improve cadence. The observations of DS2 were used to determine new times of minima. The total number of observations in both data sets included 1,563 in B, 1,986 in V, 2,858 in g', 2,767 in r', and 1,845 in i'. All images were dark current subtracted using exposures that were equal to the light frame exposures for each filter and flat field corrected. The software package MIRA (Mirametrics 2015) was used for calibration and differential aperture photometry.

The standard magnitudes of the comparison (C*) and check (K*) stars were taken from the AAVSO Photometric All-Sky Survey (APASS; Henden *et al.* 2014) data and are listed in Table 1. Figure 1 shows a finder chart for the stars in this study. The measured instrumental magnitudes for BN Ari (V*) were converted to standard magnitudes using the calibrated magnitudes of the C*. The epoch and orbital period used for all phase (Φ) calculations are 2456989.83596 and 0.29937151 day. All light curve figures are plotted from phase –0.6 to 0.6. A negative orbital phase is defined as Φ – 1. The folded light curves in standard magnitudes for each passband are shown in Figure 2. Also shown in Figure 2 is the V standard magnitude of the K* (bottom panel). The average observed K* magnitudes and errors, over all nights, are listed

Table 1. Variable (V*), comparison (C*), and check (K*) stars in this study.

Star	*R.A. (2000)* *h m s*	*Dec (2000)* ° ′ ″	*B*	*V*	*g′*	*r′*	*i′*	*(B–V)*
BN Ari (V*)	02 09 07.8	+26 29 06.0	11.35	10.54				0.81
[1]GSC1761-2281 (C*)	02 09 28.6	+26 22 32.2	12.062 ± 0.035	11.443 ± 0.055	11.690 ± 0.034	11.270 ± 0.058	11.102 ± 0.020	0.619 ± 0.062
[2]GSC1761-1732 (K*)	02 10 05.9	+26 26 44.3	12.641 ± 0.033	12.142 ± 0.071	12.329 ± 0.022	12.011 ± 0.061	11.879 ± 0.030	0.499 ± 0.078
[3]Observed check star magnitudes			12.644 ± 0.019	12.131 ± 0.016	12.330 ± 0.014	11.997 ± 0.015	11.852 ± 0.019	0.513 ± 0.024

APASS [1]comparison and [2]check star magnitudes and errors. The [3]observed check star magnitudes are the averages over all nights for each passband. The B and V magnitudes and color for BN Ari were taken from the Tycho-2 Catalog (Høg et al. *2000).*

Table 2. Available times of minima and O–C residuals from Equations (2) and (3).

Epoch HJD 2400000+	Error	Cycle	O–C Linear	O–C Quad.	References
54456.2520	0.0070	0.0	–0.0032	0.0028	Paschke 2009
54805.3150	0.0070	1166.0	–0.0073	–0.0042	Paschke 2009
54808.315	0.007	1176.0	–0.0010	0.0020	Paschke 2009
55448.8210	0.0002	3315.5	–0.0002	–0.0008	Nelson 2011
55477.8592	0.0002	3412.5	–0.0010	–0.0017	Diethelm 2011
55478.9091	0.0008	3416.0	0.0011	0.0004	Diethelm 2011
55578.3010	0.003	3748.0	0.0016	0.0006	Paschke 2012
55591.6207	0.0001	3792.5	–0.0007	–0.0018	Nelson 2012
55614.973	—	3870.5	0.0006	–0.0005	Nagai 2012
55836.6580	0.0030	4611.0	0.0011	–0.0006	Paschke 2012
55843.8416	0.0005	4635.0	–0.0002	–0.0019	Diethelm 2012
55843.9922	0.0016	4635.5	0.0007	–0.0010	Diethelm 2012
56153.5438	0.0003	5669.5	0.0022	0.0004	Hoňková *et al.* 2009
56153.5439	0.0003	5669.5	0.0023	0.0005	Hoňková *et al.* 2009
56153.5439	0.0003	5669.5	0.0023	0.0005	Hoňková *et al.* 2009
56157.5880	0.0050	5683.0	0.0049	0.0031	Paschke 2013
56251.2887	0.0001	5996.0	0.0023	0.0005	Hübscher and Lehmann 2013
56226.1419	—	5912.0	0.0027	0.0009	Nagai 2013a
56235.1228	—	5942.0	0.0025	0.0007	Nagai 2013a
56235.2722	—	5942.5	0.0022	0.0004	Nagai 2013a
56575.0589	—	7077.5	0.0023	0.0011	Nagai 2013b
56575.2082	—	7078.0	0.0019	0.0007	Nagai 2013b
56630.2929	0.0012	7262.0	0.0023	0.0012	Hübscher 2014
56630.4432	0.0010	7262.5	0.0029	0.0018	Hübscher 2014
56630.5905	0.0013	7263.0	0.0005	–0.0005	Hübscher 2014
56946.72583	0.00015	8319.0	–0.0004	–0.0002	this paper
56946.87601	0.00015	8319.5	0.0001	0.0003	this paper
56948.82148	0.00017	8326.0	–0.0004	–0.0001	this paper
56948.67210	0.00017	8325.5	–0.0001	0.0002	this paper
56949.71959	0.00010	8329.0	–0.0004	–0.0001	this paper
56949.86961	0.00019	8329.5	–0.0001	0.0002	this paper
56951.81525	0.00014	8336.0	–0.0003	–0.0001	this paper
56951.66573	0.00014	8335.5	–0.0002	0.0001	this paper
56952.71329	0.00012	8339.0	–0.0004	–0.0001	this paper
56952.86328	0.00011	8339.5	–0.0001	0.0002	this paper
56954.80871	0.00010	8346.0	–0.0006	–0.0003	this paper
56954.65938	0.00012	8345.5	–0.0002	0.0000	this paper
56956.60579	0.00021	8352.0	0.0003	0.0005	this paper
56956.90428	0.00013	8353.0	–0.0006	–0.0003	this paper
56956.75511	0.00021	8352.5	–0.0001	0.0002	this paper
56957.80245	0.00014	8356.0	–0.0006	–0.0003	this paper
56957.65326	0.00021	8355.5	–0.0001	0.0002	this paper
56960.79609	0.00008	8366.0	–0.0006	–0.0003	this paper
56960.64678	0.00013	8365.5	–0.0003	0.0000	this paper
56962.59219	0.00013	8372.0	–0.0008	–0.0005	this paper
56962.74228	0.00013	8372.5	–0.0004	–0.0001	this paper
56962.89156	0.00013	8373.0	–0.0008	–0.0005	this paper
56970.67513	0.00007	8399.0	–0.0009	–0.0005	this paper
56970.82509	0.00010	8399.5	–0.0006	–0.0002	this paper
56971.72336	0.00005	8402.5	–0.0004	–0.0001	this paper
56980.85349	0.00010	8433.0	–0.0011	–0.0007	this paper
56980.70501	0.00010	8432.5	0.0001	0.0005	this paper
56981.60284	0.00010	8435.5	–0.0002	0.0002	this paper
56985.64357	0.00006	8449.0	–0.0010	–0.0006	this paper
56985.79356	0.00006	8449.5	–0.0007	–0.0003	this paper
56987.58979	0.00010	8455.5	–0.0007	–0.0002	this paper
56988.63706	0.00010	8459.0	–0.0012	–0.0008	this paper
56988.78722	0.00010	8459.5	–0.0007	–0.0003	this paper
56989.83464	0.00004	8463.0	–0.0011	–0.0007	this paper
57270.79407	0.00006	9401.5	–0.0018	0.0003	this paper
57278.72655	0.00006	9428.0	–0.0027	–0.0005	this paper

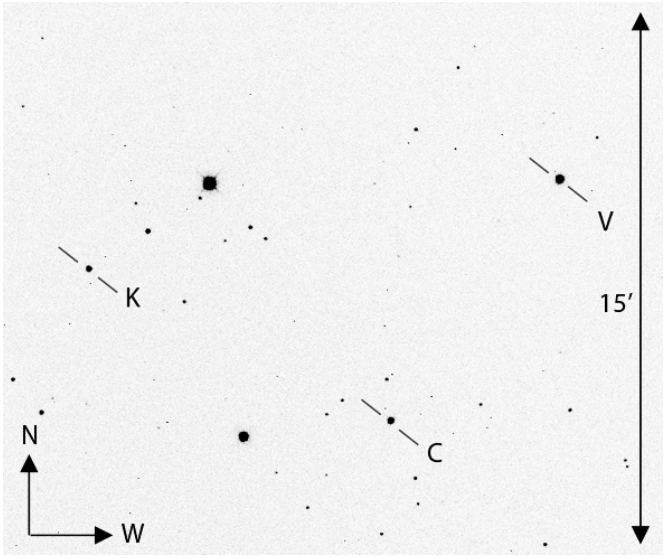

Figure 1. Finder chart for BN Ari (V), comparison (C), and check (K) stars.

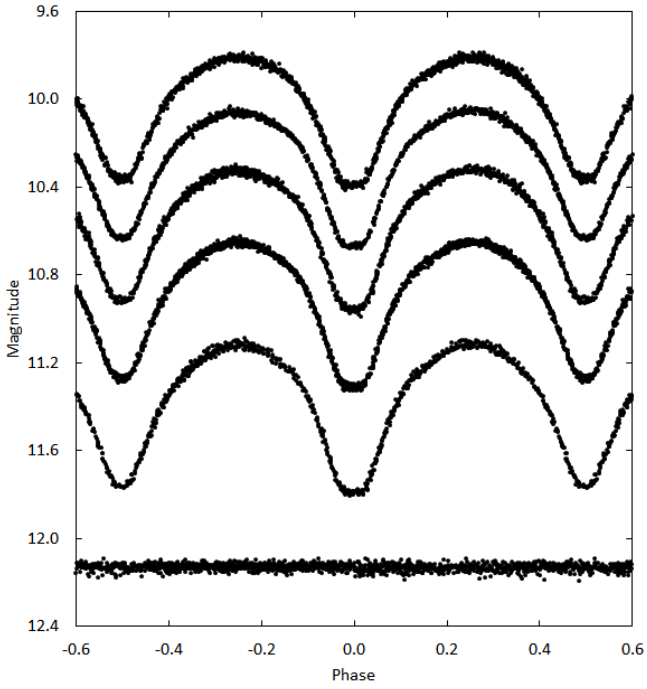

Figure 2. Folded light curves for each observed passband. The differential magnitudes of the variable were converted to standard magnitudes using the comparison star's calibrated magnitudes. From top to bottom the light curve passbands are Sloan i', Sloan r', Johnson V, Sloan g', and Johnson B. The bottom panel shows the standard V magnitudes of the check star. The standard deviations of the check star magnitudes (all nights) are shown in Table 1. Error bars are not shown for clarity.

in Table 1. These magnitudes compare well with the APASS all-sky photometry. Inspection of the K* light curves for each bandpass showed no significant variability over the two months of observation. All the observations in this study can be accessed from the AAVSO International Database (Kafka 2015).

3. Analysis

3.1. Period analysis and ephemerides

Heliocentric Julian Dates (HJD) of the new times of minima were calculated from the observations using the Kwee and van Woerden (1956) method. Time of minima from differing passbands on the same dates were compared and no significant offsets were observed. For each data set the times of minimum from DS1 were formed by averaging together the times from each passband. The new time of minima and errors are reported in Table 2 along with all available minima from other observers. The initial linear ephemeris used in this period study was taken from Paschke (2009) and is given by

$$\text{HJD Min I} = 2451525.671 + 0.299375\ E. \quad (1)$$

The O–C residuals from Equation 1 were used to calculate an improved linear ephemeris by least-squares solution and is given by

$$\text{HJD Min I} = 2456989.83596(73) + 0.29937145(10)\ E. \quad (2)$$

Figure 3 shows the residuals from Equation 1 and the best-fit linear line (solid line on figure) of Equation 2. The O–C diagram from Equation 2 is shown in Figure 4. The general trend of the O–C data indicates the period of BN Ari is continuously decreasing. A least-squares solution of the residuals from Equation 2 yields the following quadratic ephemeris:

$$\text{HJD Min I} = 2457278.77826(73) + 0.29937396(28)\ E - 1.73(16) \times 10^{-9}\ E^2. \quad (3)$$

From this solution the rate of period change was determined to be $dP/dt = -6.20\ (0.70) \times 10^{-7}$ d yr^{-1}. As can be seen in Figure 4, this ephemeris describes the data reasonably well (solid line in the figure).

3.2. Temperature, spectral type

No spectroscopic data were available for BN Ari, therefore the effective temperature and spectral type were estimated from the (B–V) color index. All DS1 B and V observations were binned with a phase width of 0.005. Both phase and magnitude were averaged in each bin interval. The binned V magnitudes were subtracted from the linearly interpolated binned B magnitudes at quadrature ($\Phi = \pm 0.25$), which gave a (B–V) value of 0.816 ± 0.005. Figure 5 shows the binned V-magnitude light curve and the bottom panel the color index. The color index at primary eclipse ($\Phi = \pm 0.025$) was also determined, giving a value of 0.832 ± 0.013. This value was corrected for interstellar extinction using galactic coordinates and a map of dust reddening (Schlafly *et al.* 2014; http://faun.rc.fas.harvard.edu/eschlafly/2dmap/querymap.php). The color

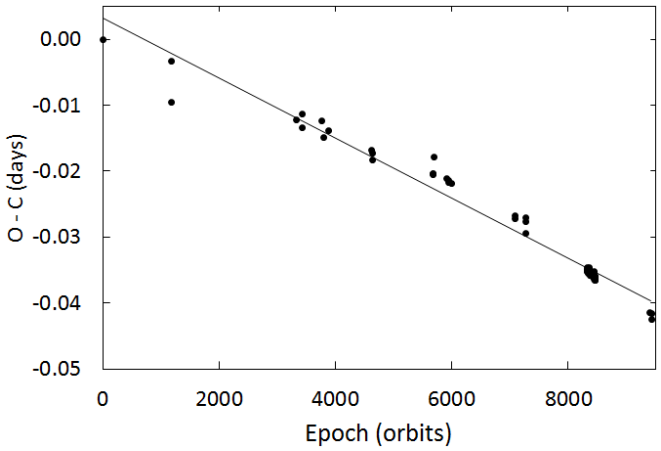

Figure 3. O–C residuals from Equation 1 with the solid line the linear ephemeris fit of Equation 2.

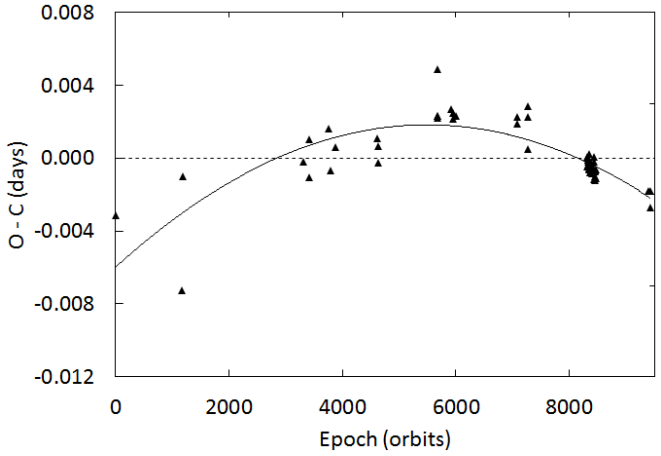

Figure 4. O–C residuals from Equation 2 with the solid line the quadric ephemeris fit of Equation 3.

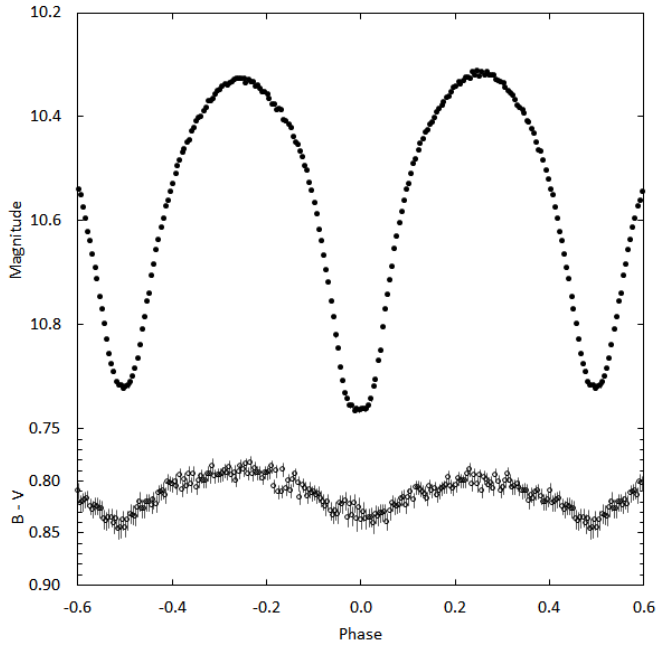

Figure 5. Light curve of all V-band observations in standard magnitudes (top panel). The observations were binned with a phase width of 0.005. The errors for each binned point are smaller than the plotted points. The B-V colors were calculated by subtracting the binned V magnitudes from the linearly interpolated binned B magnitudes.

excess is E(B–V) = 0.115 ± 0.032. The intrinsic color of the larger cooler star is thus $(B–V)_o = 0.715 \pm 0.082$. Using Table 5 of Pecaut and Mamajek (2013) gives an effective temperature of $T_{eff} = 5527 \pm 217$K and a spectral type of G7. This value was used for the effective temperature of the secondary component in the light curve analysis of section 3.3.

3.3. Synthetic light curve modeling

For light curve modeling only DS1 observations were used. These data were binned in both phase and magnitude with a phase interval of 0.01. The average number of observations per bin was 11. The binned magnitudes were converted to relative flux for modeling. For preliminary solutions BM3 was used to fit each curve individually. Standard convective parameters and limb darkening coefficients from Van Hamme's (1993) tabular values for the spectral type were used. The BM3 light curve fits for each color were consistent. The values from the V light curve fit were used as the initial input parameters for computation of a simultaneous five-color light curve solution with the WD program. In this analysis Mode 3 (the contact configuration) was used assuming a common convective envelope in direct thermal contact. The Method of Multiple Subsets (MMS) (Wilson and Biermann 1976) was employed to minimize strong correlations of the parameters. A Kurucz stellar atmosphere model was applied and the fixed inputs included standard convective parameters: gravity darkening, g1 = g2 = 0.32 (Lucy 1968), and albedo value A1 = A2 = 0.5 (Ruciński 1969). The temperature of the cooler star, T_2, was fixed at the value determined in section 3.2, 5527K. Linear limb darkening coefficients were calculated by the program from tabulated values using the method of Van Hamme (1993). A q-search was not necessary given the total eclipses provide the necessary constraints for determining the mass ratio (q). No third light was noted when included in the adjustable parameters. Only negligible small values resulted, indicating no appreciable contribution to the system's light. The solution's adjustable parameters include the inclination (i), mass ratio ($q = M_2 / M_1$), potential (Ω), temperature of the primary star (T_1), and the normalized flux for each wavelength (L). The best-fit solution parameters with errors are shown in column 3 of Table 3. The fill-out parameter was computed using a modification of the parameter defined by Lucy and Wilson (1979) and is given by

$$f = \frac{(\Omega_{inner} - \Omega)}{(\Omega_{inner} - \Omega_{outer})}, \quad (4)$$

where Ω_{inner} and Ω_{outer} are the inner and outer critical equipotential surfaces that pass through the Lagrangian points L1 and L2 and Ω is the equipotential surface which describes the stellar surface. For this solution $\Omega_{inner} = 6.214$, $\Omega_{outer} = 5.600$, and $\Omega = 6.120$ gives a fill-out value of f = 0.15. The best-fit solution with this fill-out value is consistent with a contact binary. Figure 6 shows the normalized light curves for each passband, overlaid by the synthetic solution curves. The residuals for each passband are shown in Figure 7.

Table 3. BN Ari synthetic light curve solutions.

Parameter	*Symbol*	*Solution (no spots)*	*Solution (with spots)*
Gravity Darkening	$g_1 = g_2$	0.32	0.32
Bolometric Albedo	$A_1 = A_2$	0.5	0.5
Inclination(°)	(°)	82.41 ± 0.11	82.23 ± 0.10
Effective Temperature	T_1, T_2 (K)	5731 ± 3, 5527	5728 ± 3, 5527
Surface Potential	$\Omega_1 = \Omega_2$	6.120 ± 0.006	6.114 ± 0.004
Mass Ratio	$q(M_2 / M_1)$	2.699 ± 0.004	2.685 ± 0.002
Fill-outs	$F_1 = F_2$	0.15	0.13
Luminosity	$L_1/(L_1 + L_2)B$	0.3449 ± 0.0005	0.3454 ± 0.0006
	$L_1/(L_1 + L_2)V$	0.3314 ± 0.0004	0.3312 ± 0.0004
	$L_1/(L_1 + L_2)g'$	0.3395 ± 0.0005	0.3391 ± 0.0005
	$L_1/(L_1 + L_2)r'$	0.3252 ± 0.0004	0.3251 ± 0.0004
	$L_1/(L_1 + L_2)I'$	0.3200 ± 0.0003	0.3200 ± 0.0003
Limb Darkening	x_{1B}, x_{2B}	0.813, 0.839	0.813, 0.839
	x_{1V}, x_{2V}	0.674, 0.700	0.674, 0.700
	$x_{1g'}$, $x_{2g'}$	0.763, 0.790	0.763, 0.789'
	$x_{1r'}$, $x_{2r'}$	0.603, 0.630	0.603, 0.630
	$x_{1i'}$, $x_{2i'}$	0.508, 0.532	0.509, 0.532
	$\sum res^2$	0.01416	0.00627
Spot 1 on Star 1			*Hot Spot*
Colatitude	(°)		92 ± 19
Longitude	(°)		9 ± 8
Spot Radius	(°)		15 ± 6
Spot T-factor	(T_{spot} / T_{eff})		1.11 ± 0.05
Spot 2 on Star 2			*Cool Spot*
Colatitude	(°)		39 ± 9
Longitude	(°)		299 ± 4
Spot Radius	(°)		18 ± 9
Spot T-factor	(T_{spot} / T_{eff})		0.95 ± 0.06

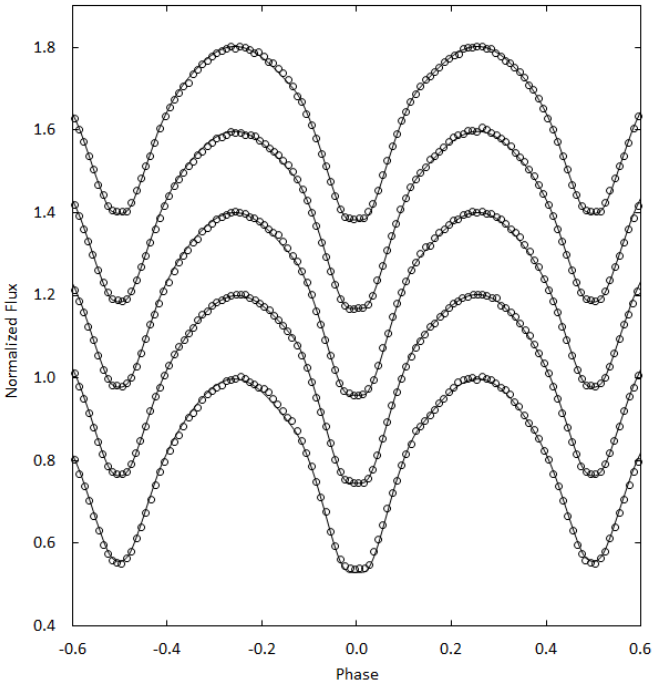

Figure 6. The WD model fit (solid curve) to the observed normalized flux curves for each passband (model without spots). From top to bottom the passbands are Sloan i', Sloan r', Johnson V, Sloan g', and Johnson B. Each curve is offset by 0.2 for this combined plot. The best-fit parameters are given in column 3 of Table 3. Error bars are omitted from the points for clarity.

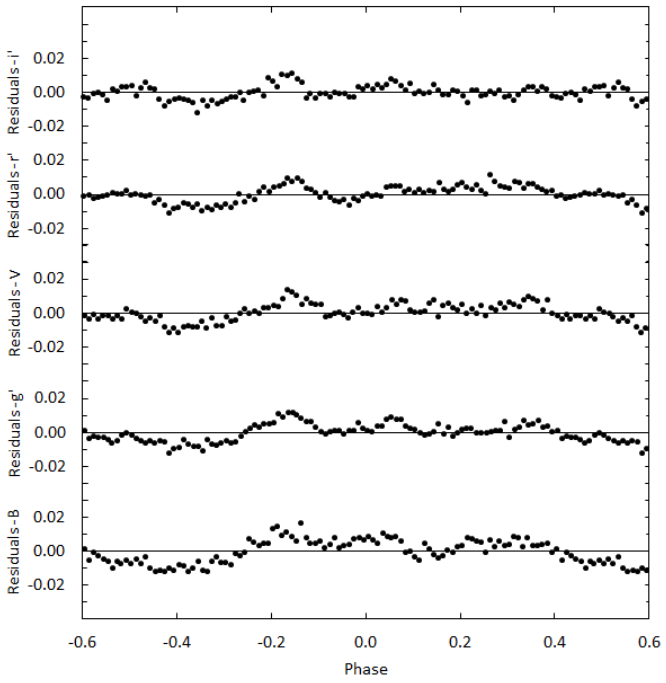

Figure 7. The residuals for the best-fit WD model without spots. Error bars are omitted from the points for clarity.

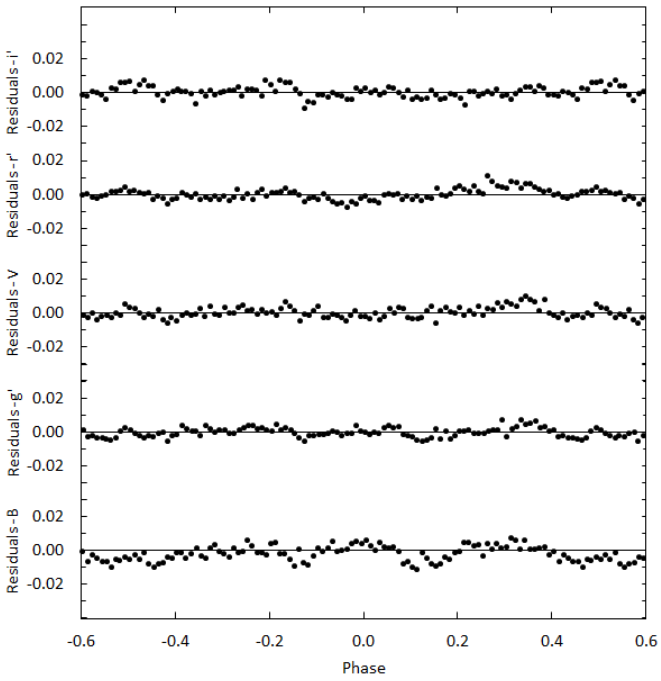

Figure 9. The residuals for the best-fit WD model with spots. Error bars are omitted from the points for clarity.

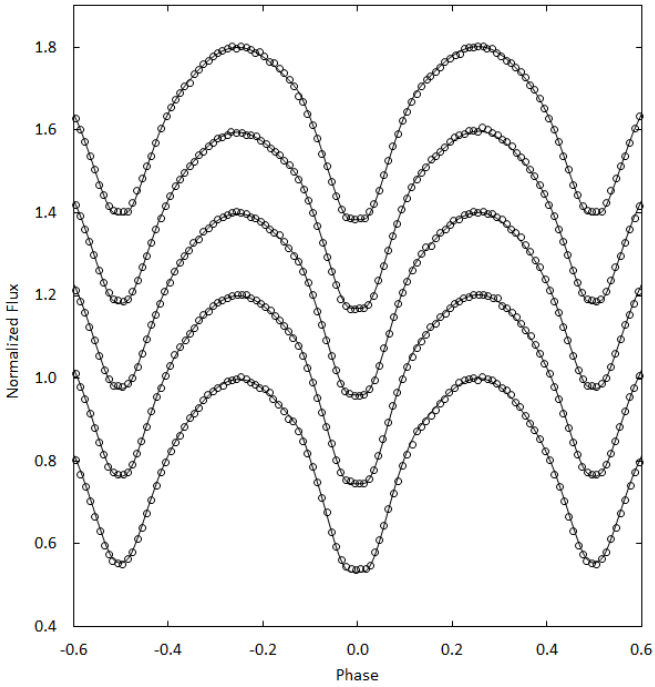

Figure 8. The WD model fit (solid curve) to the observed normalized flux curves for each passband (model with spots). From top to bottom the passbands are Sloan i', Sloan r', Johnson V, Sloan g', and Johnson B. Each curve is offset by 0.2 for this combined plot. The best-fit parameters are given in column 4 of Table 3. Error bars are omitted from the points for clarity.

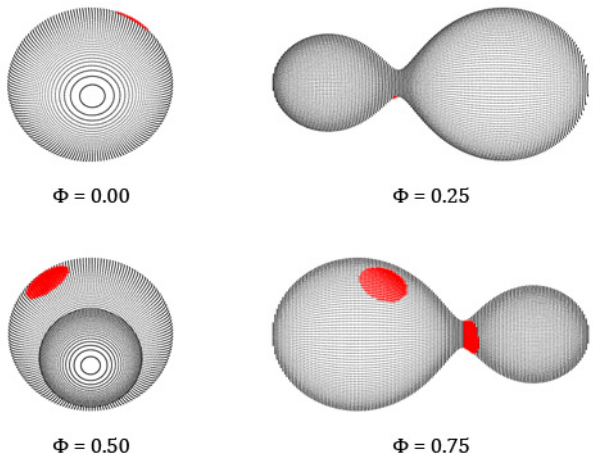

Figure 10. Roche Lobe surfaces of the best-fit WD spot model of BN Ari (orbital phase shown below each diagram).

3.4. Spot model

Figures 6 and 7 show the model light curves do not accurately reproduce the observed light curves in the phase range of 0.40 to 0.90. To improve the fit it was necessary to incorporate two star spots into the model. BM3 was used initially to manually adjust the latitude, longitude, size, and temperature of each spot until a reasonable fit was made between the synthetic and observed curves. The resulting spot parameters were then included in the first best-fit model and a new solution was attempted using the WD program. The stellar parameters were held fixed with only the spot parameters adjusted until the solution converged. Following that convergence the spot parameters were held fixed and the stellar parameters were adjusted. This was repeated until the model converged to a final solution. Column 4 in Table 3 shows the final best-fit stellar model with spots. Figure 8 shows the final model fit (solid line) to the observed light curve for each passband and Figure 9 shows the residuals for the spotted model. The sum of the residuals squared was 0.00627 for the spotted model and 0.01416 for the unspotted model (2.26 times

Table 4. Absolute parameters for BN Ari.

Parameter	*Symbol*	*Value*
Stellar masses	M_1 ($M_\odot$)	0.36
	M_2 ($M_\odot$)	0.98
Stellar radii	R_1 ($R_\odot$)	0.64
	R_2 ($R_\odot$)	0.99
Bolometric magnitude	$M_{bol,1}$	5.76
	$M_{bol,2}$	4.96
Semi-major axis	a ($R_\odot$)	2.08

larger). A graphical representation of this solution is shown in Figure 10.

4. Discussion and conclusions

Spectroscopic data are not available for this system but the absolute mass of the more massive secondary star can be estimated (M2 in this study) using the orbital period. From a statistical study of contact systems Qian (2003) found the mass is given by

$$M_2 = 0.391(\pm 0.059) + 1.96(\pm 0.17)P. \quad (5)$$

Using Equation 5 gives a mass of $M_2 = 0.98 \pm 0.08\ M_\odot$ for the secondary star and this value combined with the mass ratio (q) gives a mass of $M_1 = 0.36 \pm 0.08\ M_\odot$ for the primary component. Applying Kepler's Third Law gives the distance between the stars mass centers of $2.08 \pm 0.01\ R_\odot$. These values, stellar radii, and bolometric magnitudes are collected in Table 4.

A distance estimate to BN Ari can be found using an empirical formula derived by Ruciński and Duerbeck (1997) based on a luminosity calibration for contact binaries (using HIPPARCOS parallaxes). The absolute visual magnitude with an accuracy of ±0.22 is given by

$$M_v = -4.44 \log_{10}(P) + 3.02\,(B-V)_o + 0.12. \quad (6)$$

Using Equation 6 gives a distance modulus of (m–M) = 5.99 ± 0.25 after accounting for the extinction ($A_v = 0.358$) from the color excess found in section 3.2. This distance modulus gives a value of 158 ± 19 pc for the distance. An additional determination of distance can be made using the bolometric magnitudes in Table 4 combined with the bolometric corrections from Pecaut and Mamajek (2013). The correction for the primary star is $BC_1 = -0.12$ and $BC_2 = -0.16$ for the secondary star. The calculated magnitude for the system is $M_v = 4.69$, giving a distance of 152 pc. The two distance determinations differ by less than 5%.

The orbital period of this system appears to be changing rapidly. Magnetic braking could explain a decreasing orbital period for this pair of solar type stars but the rapid period change combined with the contact configuration may indicate conservative mass exchange. In this case the decreasing orbital period would result from mass transfer from the larger more massive star to its smaller hotter companion. The mass transfer rate can be calculated using the rate of period change and the estimated stellar masses using the following equation:

$$\frac{dM}{dt} = \frac{\dot{P} M_1 M_2}{3P(M_1 - M_2)}, \quad (7)$$

This gives a value of $1.01(0.06) \times 10^{-9}\ M_\odot$/day. There is another possible cause for the observed period change that should be considered. Light time effects caused by orbital motion around a third body may be causing an apparent orbital period change. The observed period change curve in Figure 4 may only be a small part of a sinusoidally varying ephemeris. Due to the limited number of cycles observed this model cannot be confirmed at this time. Additional observations by dedicated observers over many years may be necessary to confirm the changing period presented here and its cause.

BN Ari is a W UMa system with total eclipses and a spectral type of approximately G7. The surface temperatures of the component stars differ by 201K, which may indicate poor thermal contact. The fill-out factor of F = 0.13 indicates a contact system. A spectroscopic study of this system would be invaluable in constraining the stellar masses and spectral types.

5. Acknowledgements

The author wishes to thank Dr. Norman Markworth for the many discussions and guidance in the use of the WD program. This research was made possible through the use of the AAVSO Photometric All-Sky Survey (APASS), funded by the Robert Martin Ayers Sciences Fund.

References

Bradstreet, D. H., and Steelman, D. P. 2002, *Bull. Amer. Astron. Soc.*, **34**, 1224.

Diethelm, R. 2011, *Inf. Bull. Var. Stars*, No. 5960, 1.

Diethelm, R. 2012, *Inf. Bull. Var. Stars*, No. 6011, 1.

Henden, A. A., *et al.* 2014, AAVSO Photometric All-Sky Survey, data release 8 (http://www.aavso.org/apass).

Høg, E., *et al.* 2000, The Tycho-2 Catalogue of the 2.5 Million Brightest Stars, *Astron. Astrophys.*, **355**, L27.

Hoňková, K., *et al.* 2009, *Open Eur. J. Var. Stars*, No. 160 (*B.R.N.O. Contributions*, No.38; http://var.astro.cz/oejv/oejv.php?oejv=160).

Hübscher, J. 2014, *Inf. Bull. Var. Stars*, No. 6118, 1.

Hübscher, J., and Lehmann, P. B. 2013, *Inf. Bull. Var. Stars*, No. 6070, 1.

Kafka, S. 2015, observations from the AAVSO International Database (https://www.aavso.org/aavso-international-database).

Kwee, K. K., and van Woerden, H. 1956, *Bull. Astron. Inst. Netherland*s, **12**, 327.

Lucy, L. B. 1968, *Astrophys. J.,* **151**, 1123.

Lucy, L. B., and Wilson, R. E. 1979, *Astrophys. J.*, **231**, 502.

Mirametrics. 2015, Image Processing, Visualization, Data Analysis (http://www.mirametrics.com).

Nagai, K. 2012, *Var. Star Obs. League*, No. 53, 1.

Nagai, K. 2013a, *Var. Star Obs. League*, No. 55, 1.

Nagai, K. 2013b, *Var. Star Obs. League*, No. 56, 1.

Nelson, R. H. 2011, *Inf. Bull. Var. Stars*, No. 5966, 1.

Nelson, R. H. 2012, *Inf. Bull. Var. Stars*, No. 6018, 1.

Otero, S. A., Wils, P., and Dubovsky, P. A. 2004, *Inf. Bull. Var. Stars*, No. 5570, 1.
Paschke, A. 2009, *Open Eur. J. Var. Stars*, No. 116, 1.
Paschke, A. 2012, *Open Eur. J. Var. Stars*, No. 142, 1.
Paschke, A. 2013, *Open Eur. J. Var. Stars*, No. 155, 1.
Pecaut, M. J., and Mamajek, E. E. 2013, *Astrophys. J., Suppl. Ser.*, **208**, 9.
Pojmański, G., Pilecki, B., and Szczygiel, D. 2005, *Acta Astron.*, **55**, 275.
Qian, S. 2003, *Mon. Not. Roy. Astron. Soc.*, **342**, 1260.
Ruciński, S. M. 1969, *Acta Astron.*, **19**, 245.
Ruciński, S. M., and Duerbeck, H. W. 1997, *Publ. Astron. Soc. Pacific*, **109**, 1340.
Schlafly, E. F., *et al.* 2014, *Astrophys. J.*, **789**, 15.
Van Hamme, W. 1993, *Astron. J.*, **106**, 2096.
Van Hamme, W., and Wilson, R. E. 1998, *Bull. Amer. Astron. Soc.*, 30, 1402.
Wilson, R. E. 1990, *Astrophys. J.*, **356**, 613.
Wilson, R. E. 1994, *Publ. Astron. Soc. Pacific*, **106**, 921.
Wilson, R. E., and Biermann, P. 1976, *Astron. Astrophys.*, **48**, 349.
Wilson, R. E., and Devinney, E. J. 1971, *Astrophys. J.*, **166**, 605.
Wozniak, P. R., *et al.* 2004, *Astron. J.*, **127**, 2436.